

Enantioselective Epoxidation of Styrene by Manganese Chiral Schiff Base Complexes Immobilized on MCM-41

Moon Mandal,^[a] Vemu Nagaraju,^[b] Bipul Sarma,^[a] G. V. Karunakar,^[b] and Kusum K. Bania*^[a]

Two chiral Mn^{III} complexes synthesized and characterized by single-crystal X-ray diffraction were grafted onto mesoporous silica MCM-41. The MCM-41-immobilized solid chiral catalysts were characterized by various spectrochemical and physicochemical methods (XRD, FTIR, ²⁹Si NMR, TGA, UV/Vis/DRS, EPR, cyclic voltammetry, SEM, BET). Both the homogeneous and heterogeneous Mn^{III} chiral complexes are found to be effective

catalysts for epoxidation of styrene. MCM-41-supported chiral catalysts are found to retain their catalytic activity up to five cycles. When an ionic liquid was implemented to enhance the catalytic recyclability of the homogeneous catalysts, they can be recycled up to three times. However, after the third cycle the catalytic activities of the complexes were found to decrease due to rupturing of the chiral catalyst.

Introduction

Chiral Schiff base transition-metal complexes are highly attractive catalysts for the synthesis of enantomerically enriched chiral compounds.^[1–4] Of the various transition-metal catalysts, Schiff base complexes of Mn^{III/IV} have drawn the attention of researchers not only because of their ability to effect various oxidation processes^[5,6] but also for their role in biological processes.^[7] Jacobsen and Katsuki first reported the enantioselective epoxidation of unfunctionalized alkenes using chiral manganese salen catalysts.^[8,9] Since then chiral Mn Schiff base complexes have been used for the epoxidation of various alkenes and for ring-opening reactions.^[10–12] Although homogeneous chiral Mn Schiff base complexes have been found to be effective for asymmetric epoxidation still they have certain limitations. Homogeneous catalysts fail in terms of reusability and recovery, which prevents their commercial application. Besides the difficulty that lies in their recovery, chiral Schiff base complexes may lose their catalytic ability because of demetalation and ligand degradation due to oxidation or reduction.^[13,14,15] Recently, we have reported a stepwise loss of catalytic ability of a chiral Cu^{II} Schiff base complex in asymmetric Henry reaction.^[16]

Owing to fatal disadvantages in homogeneous catalysis, researchers and scientists have developed alternative strategies

to restore the catalytic activity of the chiral catalyst. Since chiral metal catalysts are expensive, they must be preserved for longer periods of time and recycled.^[17,18] Recent articles on the design of reusable chiral salen complex suggest that the use of inorganic mantles such as microporous and mesoporous materials (e.g. zeolites, MCM-41, LDH etc.) can be convenient for retaining the catalytic activity of these catalysts.^[19–23] Among the different inorganic supports, MCM-41 has well-ordered pore arrays, large surface area, uniform pore size distribution, and tunable pore diameter (4–15 nm).^[24] Because of these unique properties MCM-41 has been extensively used for the immobilization of chiral metal catalysts.^[25,26] Various research groups have reported on the successful immobilization of chiral Schiff base complexes on MCM-41 and their catalytic application in various asymmetric epoxidation reactions.^[27,28]

In this current work we have synthesized two chiral Mn^{III} Schiff base complexes and immobilized them on MCM-41 (Scheme 1). The two chiral catalysts are found to be effective for the asymmetric epoxidation of styrene. The catalytic activities of the two complexes are found to be different owing to their structural difference. MCM-41-immobilized chiral catalyst has enhanced catalytic activity in comparison to the homogeneous analogues. Moreover, heterogeneous systems are found to be more suitable in terms of recyclability and stability.

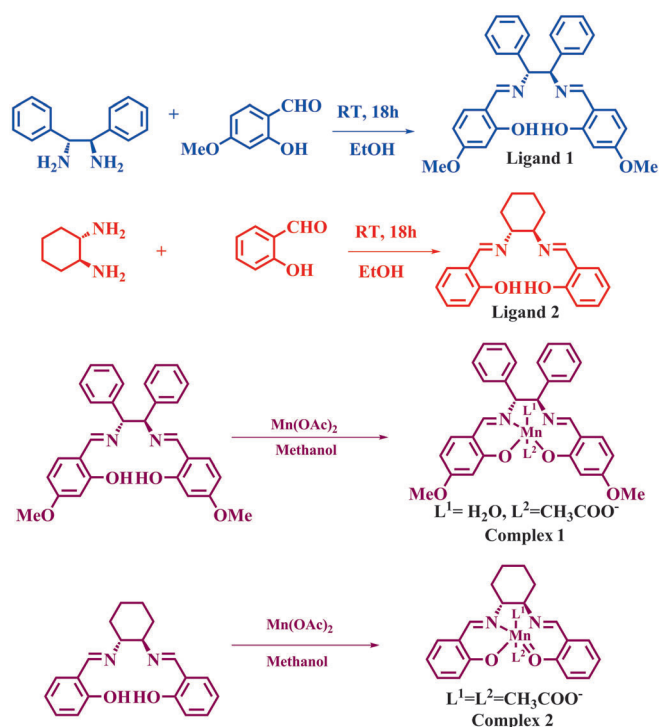
Results and Discussion

The synthesized materials were characterized by using various spectrochemical and physicochemical techniques. The structures of the synthesized Mn^{III} complexes were confirmed by single-crystal XRD analysis. Immobilized chiral catalysts were characterized by powder X-ray diffraction (PXRD), fourier transform infra-red (FTIR), Brunauer–Emmet–Teller (BET), ultraviolet/visible/diffuse reflectance spectroscopy (UV/Vis/DRS), cyclic voltammetry, scanning electron microscopy (SEM), and thermogravimetric analysis (TGA), details of which are described below

[a] M. Mandal, Dr. B. Sarma, Dr. K. K. Bania
Department of Chemical Sciences
Tezpur University
Napaam, Assam 784028 (India)
E-mail: kusum@tezu.ernet.in

[b] V. Nagaraju, Dr. G. V. Karunakar
Division of Crop Protection Chemicals
Indian Institute of Chemical Technology
Uppal Road, Hyderabad, Andhra Pradesh 500607 (India)

Supporting information for this article (including details of materials used and physical measurement implemented, H-bond matrices, FTIR spectra of complex 1 and complex 2, and UV/Vis spectra of complex 1 and complex 2 after three consecutive cycles) is available on the WWW under <http://dx.doi.org/10.1002/cplu.201402446>.



Scheme 1. Preparation of ligand 1 and ligand 2 and their corresponding Mn Schiff base complexes.

separately. After characterizing the materials, we studied the epoxidation of styrene using synthesized chiral homogeneous and heterogeneous catalysts. These results are presented after a description of the material characterization.

Single-crystal X-ray diffraction study of manganese Schiff base complexes

Purple needle-shaped crystals of complex 1 and complex 2 were obtained from acetonitrile. The crystallographic parameters of the two complexes are summarized in Table 1. Hydrogen bond distances in the X-ray crystal structures (Table S1) were neutron-normalized by fixing the D–H distance to its accurate neutron value (O–H 0.983 Å, N–H 1.009 Å, C–H 1.083 Å). The single-crystal structure of complex 1 was solved and refined in the monoclinic $P2_1$ space group. Two molecules of the complex and two molecules of water were found in each symmetry-independent unit. The Schiff base ligand binds the metal Mn at two nitrogen and two oxygen coordination sites. An acetate anion and a water molecule complete the octahedral geometry of the central metal Mn (Figure 1). The crystal structure of complex 2 consists of molecular chains running along the [001] axis connected by acetate and methanol. Two acetate anions bind three molecules of the Schiff base complex 2 in a row forming a monomeric unit (Figure 2).

In complex 1, the Mn–O distances are found to range from 1.890–1.899 Å and Mn–N distances range from 1.982–1.984 Å; the Mn–O(H₂O) and Mn–O(OOCH₃) distances are found to be 2.398 and 2.161 Å, respectively. In complex 2, the Mn–O bonds range from 1.879–1.887 Å and the Mn–N bonds are

| Table 1. Crystal data parameters for complex 1 and complex 2. | | |
|---|--|--|
| Crystal data | Complex 1 | Complex 2 |
| chemical formula | C ₆₄ H ₆₂ Mn ₂ N ₄ O ₁₆ | C ₆₇ H ₇₂ Mn ₃ N ₆ O ₁₃ |
| formula wt. | 1253.06 | 1334.13 |
| crystal system | monoclinic | orthorhombic |
| <i>T</i> [K] | 100 | 100 |
| <i>a</i> [Å] | 13.542(2) | 13.9964(8) |
| <i>b</i> [Å] | 8.9342(14) | 19.9934(11) |
| <i>c</i> [Å] | 24.371(4) | 21.4608(13) |
| α [°] | 90 | 90 |
| β [°] | 91.878(11) | 90 |
| γ [°] | 90 | 90 |
| volume [Å ³] | 2947.1(8) | 6005.5(6) |
| space group | $P2_1$ | $P2_12_12_1$ |
| <i>Z</i> | 2 | 4 |
| <i>D</i> _{calc} [g cm ⁻³] | 1.412 | 1.476 |
| μ [mm ⁻¹] | 0.503 | 0.694 |
| reflins. collected | 26 255 | 43 063 |
| unique reflins. | 10 365 | 18 126 |
| observed reflins. | 7338 | 9031 |
| <i>R</i> ₁ [<i>I</i> > 2 σ (<i>I</i>)], <i>wR</i> ₂ | 0.0490, 0.0926 | 0.0676, 0.1411 |
| GOF | 0.976 | 0.833 |
| instrument | Bruker CCD-APEX-II | Bruker CCD-APEX-II |

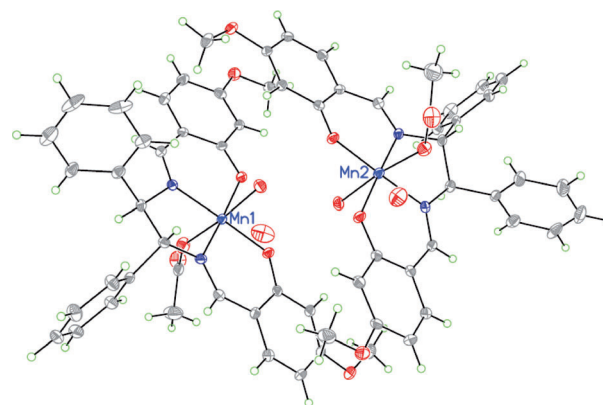


Figure 1. X-ray crystal structure of complex 1 with ellipsoids at the 35% probability level.

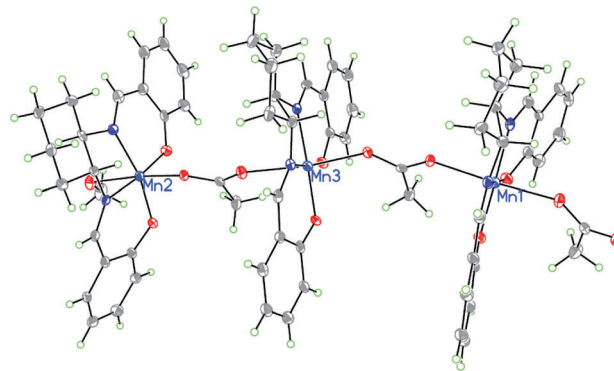


Figure 2. X-ray crystal structure of complex 2 with ellipsoids at the 35% probability level.

1.993–2.001 Å. In both complexes the Mn–O distances are found to be slightly longer than the usual due to Jahn–Teller distortion.^[29]

Powder X-ray diffraction study (PXRD)

The PXRD patterns of MCM-41, pyridine carboxaldehyde modified MCM-41, and MCM-41 with the immobilized metal complex are shown in Figure 3. MCM-41 shows one characteristic

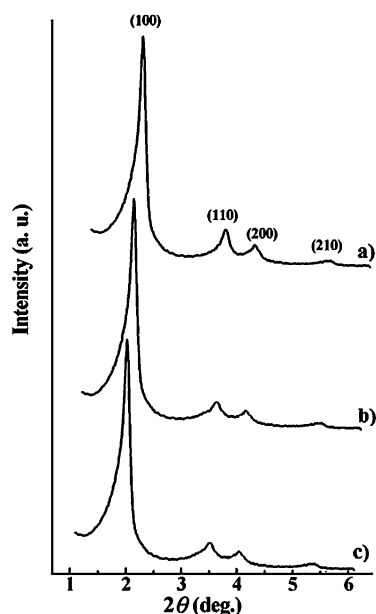


Figure 3. XRD patterns of a) MCM-41 b) pyridine carboxaldehyde modified MCM-41 c) Metal complexes immobilized on MCM-41 as stacked plots.

intense peak due to reflection at the (100) plane and two low-intensity peaks due to reflections at the (110) and (200) planes.^[27] On complexation, the intensities of all peaks decrease and the intensities of the 110 and 200 reflections decrease more on immobilization of metal complex on MCM-41, with only a minor shift in the 2θ values (Figure 3 b,c). This can be attributed to shrinkage effects due to the presence of the metal complex in the pore channels of MCM-41, causing a decrease in the pore size and an increase in the d -spacing. Nevertheless, the retention of the characteristic peaks indicates that the long-range order of mesoporous hexagonal channels is preserved upon modification. Similar shifts in the 2θ values upon immobilization of metal complexes on MCM-41 has been reported previously^[27,28] and supports the successful attachment of chiral metal catalysts to modified MCM-41.

Surface area and CHN analysis

MCM-41 and pyridine carboxaldehyde modified MCM-41 show typical type IV isotherms having three well-distinguished regions:^[30] mono- and multilayer adsorption on the pore walls (region A), capillary condensation (region B), and multilayer adsorption on the outer surface (region C) (Figure 4 top, a,b). The

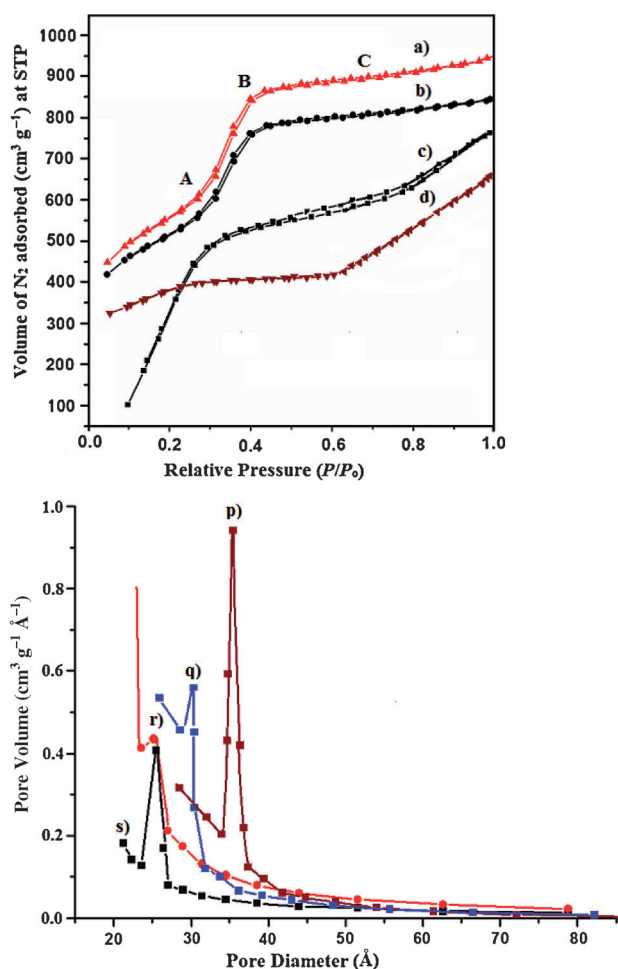


Figure 4. Top: N_2 -adsorption isotherm of a) MCM-41, b) pyridine carboxaldehyde modified MCM-41, c) complex 1/MCM-41, d) complex 2/MCM-41. Bottom: Pore size distribution in p) MCM-41, q) pyridine carboxaldehyde modified MCM-41, r) complex 1/MCM-41, s) complex 2/MCM-41.

MCM-41-immobilized catalyst shows a type III isotherm, indicating incorporation of the metal complex into the pores of MCM-41 through a multistep grafting method (Figure 4 top, c,d).^[24] This is in agreement with the decrease in the pore volume of MCM-41 after incorporation of chiral Mn^{III} Schiff base complexes. BET surface area, pore diameter, and pore volume data are presented in Table 2. The BET surface areas in functionalized MCM-41 and complex 1/MCM-41 and complex 2/MCM-41 are less than that of pure MCM-41. Similarly, pore diameters as well as pore volumes are found to be less in the case of the modified MCM-41. For example, on immobilization of complex 1, the BET surface area decreases from 1015 to 623 $m^2 g^{-1}$, the pore size from 37 to 25 Å, and the pore volume from 0.576 to 0.415 $cm^3 g^{-1}$, Figure 4 bottom, p, q, r, and s).

The amount of Mn loading in the two immobilized complexes was determined by inductively coupled plasma (ICP) spectrometer analysis. Carbon, hydrogen and nitrogen contents were determined by CHN analysis. The C/N ratio is close to that expected (Table 2). This further indicates that metal complexes are immobilized on the surface of MCM-41.

Table 2. BET and CHN analysis of MCM-41, pyridine carboxaldehyde modified MCM-41, complex 1/MCM-41, complex 2/MCM-41. Mn loading is calculated from ICP analysis.

| Compound | Mn loading [mg/100 mg] | BJH pore diameter [Å] | Total pore vol. [cm ³ g ⁻¹] | BET surface area [m ² g ⁻¹] | Elemental analysis [wt%] | | | |
|---|------------------------|-----------------------|--|--|--------------------------|------|------|------|
| | | | | | C | H | N | C/N |
| MCM-41 | – | 37 | 0.944 | 1015 | – | – | – | – |
| pyridine carboxaldehyde modified MCM-41 | – | 30 | 0.576 | 745 | 10.62 | 2.13 | 2.32 | 4.57 |
| complex 1/MCM-41 | 10.82 | 26 | 0.423 | 623 | 69.46 | 3.67 | 7.17 | 9.68 |
| complex 2/MCM-41 | 11.35 | 25 | 0.415 | 638 | 54.90 | 2.44 | 7.35 | 7.46 |

FTIR and solid-state ²⁹Si and ¹³C NMR analysis

FTIR spectra of the two Mn complexes are shown in Figure S1 and Figure S2, respectively. Both complexes show characteristic stretching vibrational bands for C=N, C=C, C–O, –CH, and =CH [$\nu(\text{C}=\text{N})$, 1600–1617 cm⁻¹], [$\nu(\text{C}=\text{C})$, 1526–1540 cm⁻¹], [$\nu(\text{C}=\text{O})$, 1304–1307 cm⁻¹], [$\nu(\text{C}=\text{H})$, 2932–2948 cm⁻¹], and [$\nu(\text{C}=\text{H})$, 762–777 cm⁻¹].^[23] The FTIR spectrum of calcined MCM-41 (Figure 5a) shows characteristic bands at 1064 and 3464 cm⁻¹ for Si–O–C–Si and Si–OH bonds, respectively.^[25] Treatment with 3-aminopropyltriethoxysilane (APTS) yields the amine-functionalized MCM-41, which shows additional bands at 3274, 2940, 1567, and 1492 due to $\nu(\text{N}=\text{H}$ stretching), $\nu(\text{C}=\text{H}$, stretching), $\nu(\text{N}=\text{H}$ bending), and $\nu(\text{CH}_2$ bending), respectively (Figure 5b). The presence of N–H stretching and –CH₂ bending modes indicates the functionalization of MCM-41 with amine via APTS. After MCM-41 had been functionalized with amino groups, it was further treated with pyridine carboxaldehyde (Scheme 2). FTIR spectrum of pyridine carboxaldehyde modified MCM-41 (Figure 5c) shows peaks at 1647, 1548, and 1393 cm⁻¹ corre-

sponding to C=N, C=C (aromatic), and C–N stretching vibrations and it does not possess any peaks due to N–H vibrations. The presence of the C=N vibrational mode and absence of N–H vibrational bands confirms the coupling of the –NH₂ group of the siloxyl moiety with the –CHO group of pyridine carboxaldehyde through formation of a C=N bond.

The formation of amino-functionalized MCM-41 and pyridine carboxaldehyde modified MCM-41 is further confirmed by ²⁹Si and ¹³C NMR spectroscopy. The ²⁹Si NMR spectrum of MCM-41 shows a broad peak at –97.3 to –99.3 ppm (Figure 6a). However, on modification with APTS this chemical shift value shifted to –110.5 ppm (Figure 6b) and upon further treatment with pyridine carboxaldehyde a downfield shift occurs (–93.3 ppm; Figure 7a). These shifts in the ²⁹Si NMR spectrum further indicates that the chemical environment near Si in MCM-41 does not remain the same upon modification. The ¹³C NMR spectrum of pyridine carboxaldehyde modified MCM-41 shows a signal at 160 ppm due to the aromatic moiety, two peaks at 23.7 and 11.9 ppm due to the aliphatic carbon atom of the aminopropyl linker, and peaks at 45.1 and 48.1 ppm due

to the carbon atom in the C=N bond (Figure 7b). These signals clearly provide the evidence for the incorporation of the linker group on the silica matrix.

The formation of linker groups on the silica matrix is thus confirmed. In the next step, the chiral Mn Schiff base complexes are anchored to MCM-41 through the formation of an Mn–N bond with the linker group (Scheme 2). The FTIR spectrum of the MCM-41-immobilized complexes shows bands similar to those of neat complexes in the region of 1600–1200 cm⁻¹. The presence of the most characteristic bands above 1600 cm⁻¹ due to the C=N bond confirms the immobilization of the metal complexes over MCM-41 (Figure 5d).

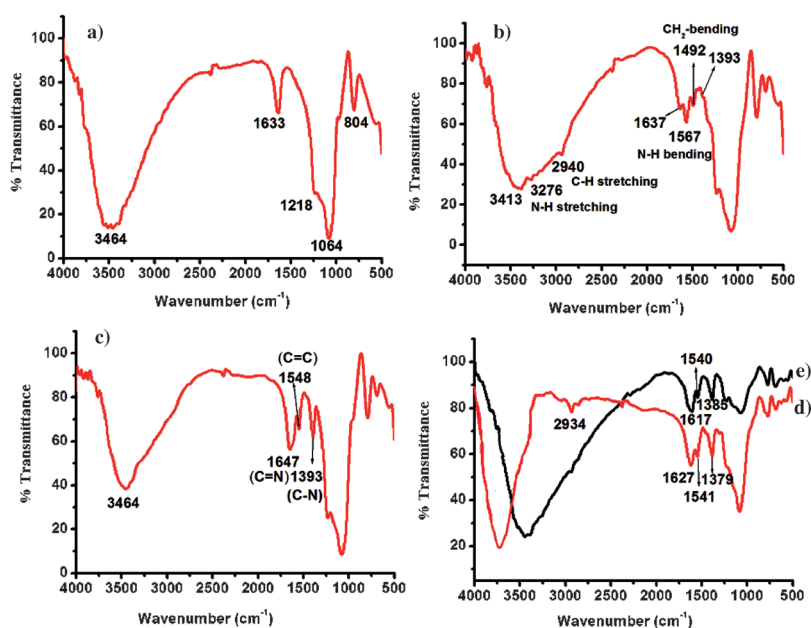
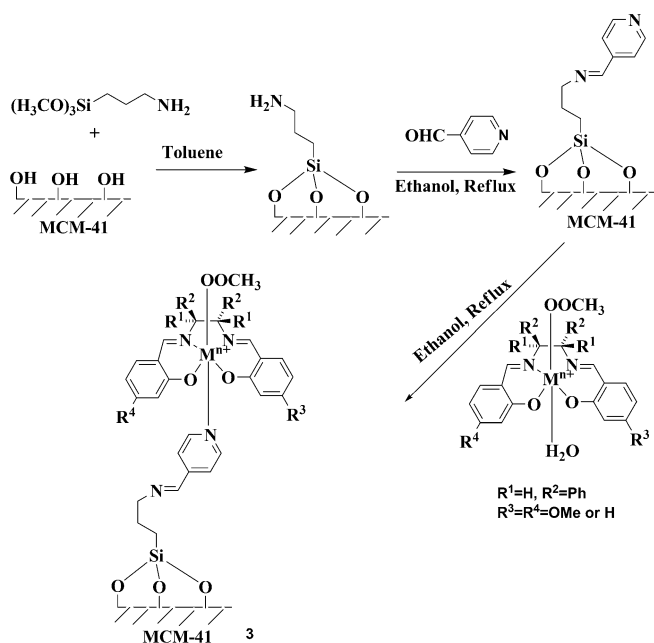


Figure 5. FTIR spectra of a) MCM-41, b) APTS-MCM-41, c) pyridine carboxaldehyde modified MCM-41, d) complex 1/MCM-41, e) complex 2/MCM-41



Scheme 2. Synthesis of MCM-41-supported Mn^{III} chiral Schiff base complex **3**.

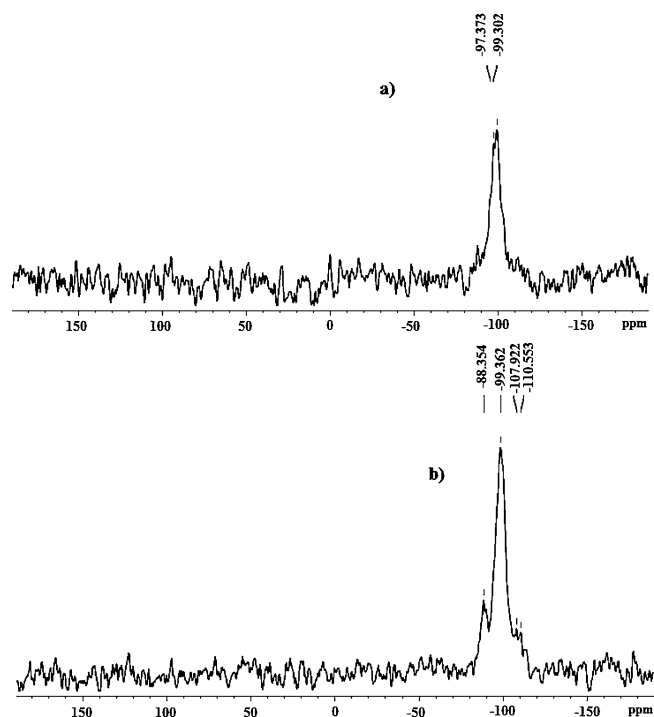


Figure 6. ²⁹Si NMR spectra of a) MCM-41, b) APTS-MCM-41.

UV/Vis and diffuse reflectance spectra

The UV/Vis spectrum of the ligands, Mn^{III} metal complexes, and MCM-41-supported metal complexes are shown in Figure 8. The transition assignment for each absorption is listed in Table 3. The UV/Vis spectra of the two ligands show character-

istics peaks due to $\pi \rightarrow \pi^*$ and $n \rightarrow \pi^*$ transitions. The bands appearing below 300 nm are due to $\pi \rightarrow \pi^*$ transitions and above 300 nm due to $n \rightarrow \pi^*$ transitions. Complex **1** shows bands at 247, 297, 334, 392, and 479 nm. The bands at 247 and 297 nm are both due to $n \rightarrow \pi^*$ transitions. The bands at 334 and 392 nm are because the metal-to-ligand charge transfer transition (MLCT) and the band at 479 nm arises from a d-d transition. The band at 479 nm is mainly a combination of a charge transfer and d-d transition band. Complex **2** shows bands at 239, 281, 307, 344, and 398 nm. The lower-wavelength bands are due to $\pi \rightarrow \pi^*$ transitions and the higher-wavelength bands are due to charge transfer transitions.

The diffuse reflectance spectra (DRS) of the MCM-41-immobilized complexes also show bands approximately in the same region (Table 3). Small changes in the wavelengths can be attributed to the effect of the MCM-41 matrix. MCM-41-anchored complex **1** shows transitions due to $\pi \rightarrow \pi^*$ and $d\pi \rightarrow p\pi$. The most significant changes observed in the case of complex **1** and complex **2** supported on MCM-41 is the appearance of a band above 600 nm. In the case of complex **1**, the band at 653 nm is due to a transition from a $d\pi$ orbital (HOMO) to a $p\pi$ orbital of the ligand (LUMO) mostly concentrated on the pyridine linkage. Complex **2**/MCM-41 shows two additional bands at 491 nm and 613 nm besides the $\pi \rightarrow \pi^*$ transition. These two transitions originate from the excitation of an electron from a $d\pi$ orbital (HOMO) to a $p\pi$ orbital (LUMO) mostly concentrated at the linker atoms of the pyridine carboxaldehyde moiety. Thus the appearance of charge transfer bands truly indicates the binding of the metal complex through pyridine carboxaldehyde with amino-functionalized MCM-41.

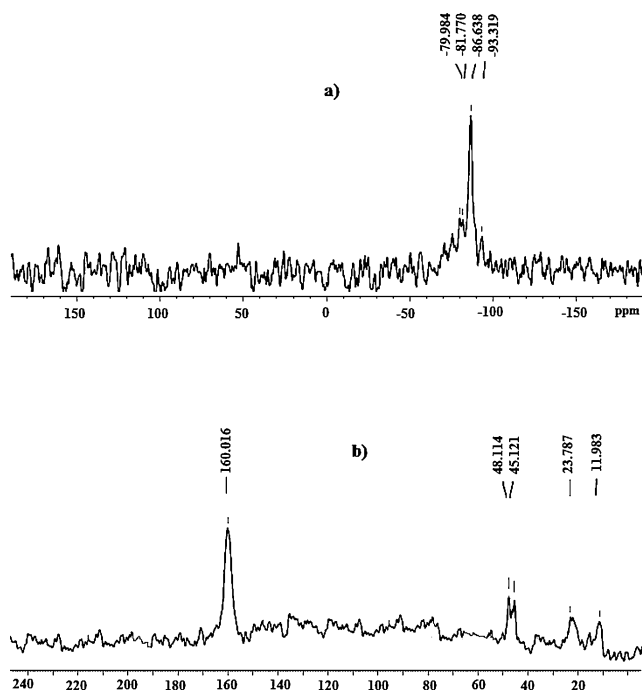


Figure 7. a) ²⁹Si NMR spectrum of pyridine carboxaldehyde modified MCM-41, b) ¹³C NMR spectrum of pyridine carboxaldehyde modified MCM-41.

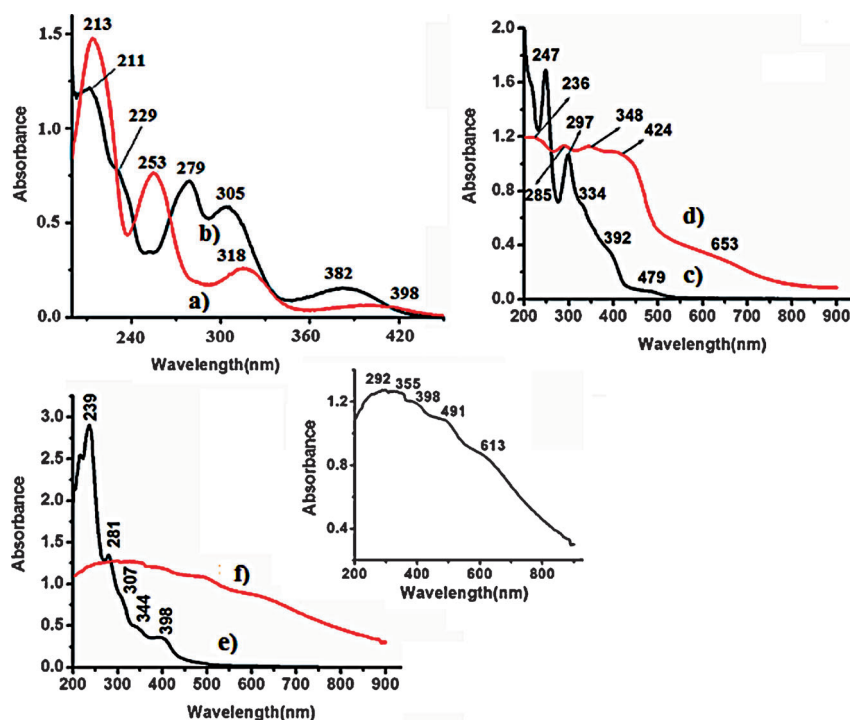


Figure 8. UV/Vis spectra of a) ligand 1, b) ligand 2, c) complex 1, d) complex 1/MCM-41, e) complex 2, f) complex 2/MCM-41 (and inset).

| Table 3. Assignment of UV/Vis transitions in synthesized complexes. | | |
|---|----------------|---|
| Compound | λ [nm] | Transition |
| ligand 1 | 213, 253 | $\pi \rightarrow \pi^*$ |
| | 318, 398 | $n \rightarrow \pi^*$ |
| ligand 2 | 211, 229, 279 | $\pi \rightarrow \pi^*$ |
| | 305, 382 | $n \rightarrow \pi^*$ |
| complex 1 | 247, 297 | $n \rightarrow \pi^*$ |
| | 334, 392 | $n \rightarrow \pi^*$ |
| | 479 | $d\pi \rightarrow p\pi^*$ |
| complex 1/MCM-41 | 236, 285 | $\pi \rightarrow \pi^*$ |
| | 348 | $n \rightarrow \pi^*$ |
| | 424 | $d\pi \rightarrow p\pi^*$ |
| complex 2 | 653 | $d\pi \rightarrow p\pi^*$ (pyridine carboxaldehyde) |
| | 239, 281 | $\pi \rightarrow \pi^*$ |
| | 307, 344 | $\pi \rightarrow \pi^*$ |
| complex 2/MCM-41 | 398 | $\pi \rightarrow \pi^*$ |
| | 292, 336 | $\pi \rightarrow \pi^*$ |
| | 355, 398 | $n \rightarrow \pi^*$ |
| | 491 | $d\pi \rightarrow p\pi^*$ |
| | 613 | $d\pi \rightarrow p\pi^*$ (pyridine carboxaldehyde) |

Cyclic voltammetry study

The voltammograms of the unsupported complexes were recorded with 0.01 M solutions of the complexes in acetonitrile using 0.1 M tetrabutyl ammonium bromide (NBu₄Br) as a supporting electrolyte. Cyclic voltammograms of the two metal complexes were recorded at different scan rates and are shown in Figure 9a,b. When the voltammograms for complex 1 and complex 2 were recorded starting from the positive

potential range 1.0 V to -1.0 V, no anodic or cathodic peak potentials were observed. However, starting from the negative potential range, we could observe a strong reduction peak at -0.415 V for complex 1 and at -0.365 V for complex 2 due to the reduction of Mn^{III} to Mn^{II}. Bonadies et al.^[31] has also observed a single irreversible reduction peak for similar complexes in acetonitrile and has attributed it to the formation of 1:1 electrolyte of [Mn^{III}(salen)]⁺ and CH₃COO⁻. Hence the presence of a single reduction peak potential confirms the initial oxidation state of the metal complexes to be +III; however, in solution the axial ligand (CH₃COO⁻) dissociates and [Mn^{III}(salen)]⁺ forms. A plot of current peak vs. the square root of the scan rate is found to be linear, indicating that this a normal diffusion-controlled

process (Figure 10a,b). The correlation is found to be much more prominent for the peak current values corresponding to the lower scan rate (Figure 10b).

For recording the cyclic voltammograms of the MCM-41-supported chiral Mn Schiff base complexes, the working electrode was prepared by taking a 1:1 weight ratio of metal complexes in 1 mL of acetonitrile.^[32] This suspension was ultrasonicated for 15 min. Then 10 μ L of this dispersion was coated on a glassy carbon electrode and 5 μ L of 5% styrene (as binder from Aldrich) was applied to this coating and dried. The glassy carbon electrode was used as the working electrode and Ag/AgCl/KCl (saturated) was used as reference electrode. Cyclic voltammograms corresponding to the MCM-41-immobilized complexes also show a single electron reduction peak due to the Mn^{III} \rightarrow Mn^{II} process (Figure 9c,d). However, the reduction potential values (-0.565 V and -0.599 V) differ from those of the homogeneous systems. The change in the peak potential values upon immobilization on the solid support may be due to the effect of the MCM-41 matrix. In the case of the immobilized system we the plot of the scan rate versus the peak current was linear, indicating a surface-controlled process (Figure 10c).

SEM analysis

Scanning electron microscopic images of MCM-41 and MCM-41-anchored salen complexes are shown in Figure 11. SEM micrographs of modified MCM-41 show no significant change in comparison to its precursor except some formation of agglomerate particles due to complex formation. This indicates that

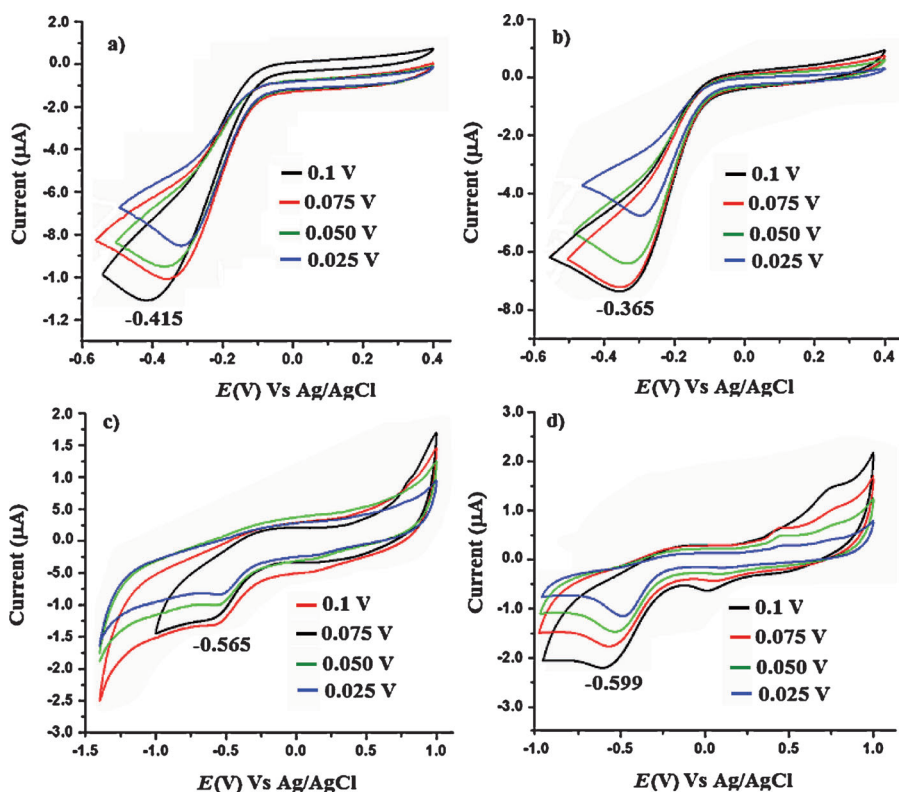


Figure 9. Cyclic voltammograms of a) complex 1, b) complex 2, c) complex 1/MCM-41, d) complex 2/MCM-41 recorded at different scan rates (0.1 V to 0.025 V).

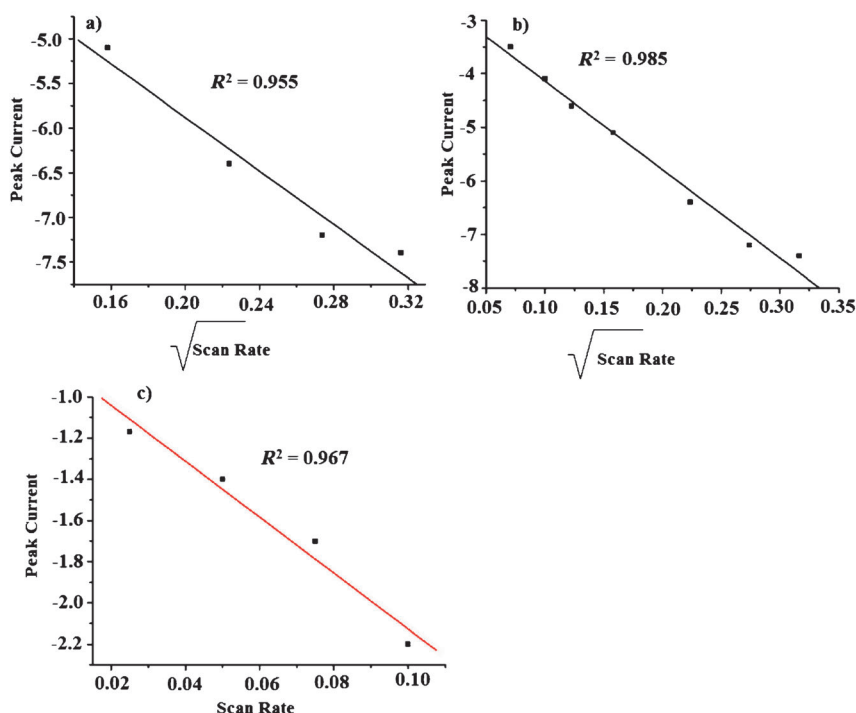


Figure 10. a) Plot of square root of scan rate (0.1 V to 0.075 V) vs. peak current (in μA). b) Plot of square root of scan rate (0.1 V to 0.005 V) vs. peak current (in μA). c) Plot of scan rate (0.1 V to 0.075 V) vs. peak current (in μA). Plots determined from the values from cyclic voltammograms of complex 1 (a and b) and complex 1/MCM-41 (c).

chiral modification of the MCM-41 surface does not lead to significant changes in the surface morphology. However, the presence of agglomerate particles indicates the presence of metal complexes which block the pores of the mesoporous system.

TGA analysis

Thermogravimetric patterns of the parent Mn Schiff base complexes and of the immobilized complexes are displayed in Figure 12. Comparison of the thermogravimetric analysis indicates that complex 1 has four weight-loss steps at about 46, 160, 288, and 394 °C while complex 2 shows four weight-loss steps at about 45, 190, 280, and 402 °C (Figure 12 top (a,b)). On the basis of the weight changes, the first weight-loss step in both complexes corresponds to the loss of a water molecule as an endothermic phenomenon. The second weight loss at 160–190 °C may be related to the loss of an acetate group. There is a sharp weight change at 394 °C (complex 1) and at 402 °C (complex 2), which is attributed to the loss of Schiff base ligands. However, for the corresponding immobilized complexes the weight loss extends up to 474 °C (Figure 12 top (c,d)), which indicates that the thermal stability is greatly enhanced. A comparison of the dTGA curve for the parent complex 1 and immobilized complex 1 clearly that immobilization enhances the thermal stability of the complexes (Figure 12 bottom (X and Y curves)). On the basis of the thermal analysis data, we may conclude that MCM-41-immobilized complexes may be treated thermally without any significant decomposition.

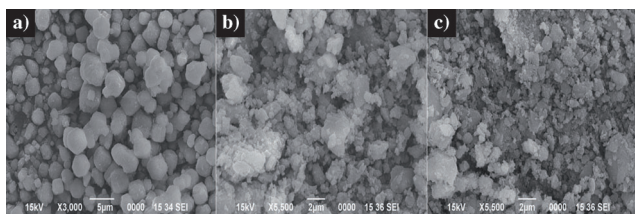


Figure 11. SEM images of a) MCM-41, b) complex 1/MCM-41, c) complex 2/MCM-41.

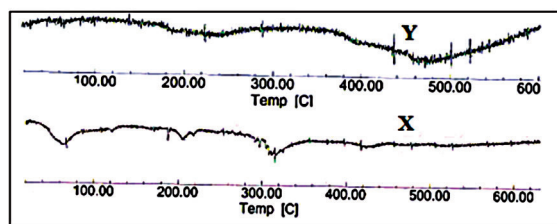
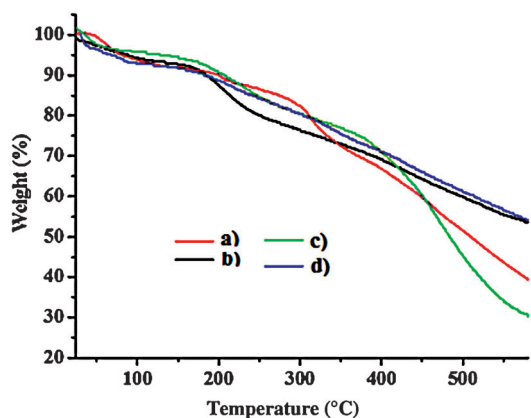


Figure 12. Top: TGA analysis of a) complex 1, b) complex 2, c) complex 1/MCM-41, d) complex 2/MCM-41. Bottom: X and Y are corresponding dTGA curves for complex 1 and complex 1/MCM-41, respectively.

Catalytic activity

As mentioned in the introduction, Mn^{III} chiral Schiff base complexes are well-known catalysts for the epoxidation of styrene. Herein we have also investigated the oxidation of styrene to styrene oxide (SO) in the presence of the synthesized homogeneous and also the MCM-41-supported metal complexes. Hydrogen peroxide (30%, H₂O₂) is used as the oxidant in the catalytic process. The catalytic oxidation of styrene is dependent on various parameters such as solvent, temperature, amount of catalyst, and oxidant. Here we discuss the effect of these parameters on the oxidation of styrene catalyzed by the chiral Mn^{III} complexes.

Effect of solvent and temperature

In order to observe the effect of the solvent on the oxidation of styrene we employed complex 1 as a test catalyst. We chose a range of solvents (both protic and aprotic) having different polarities (i.e. different dielectric constants) and the results are shown in Table 4. In the presence of highly polar solvents the

Table 4. Oxidation of styrene using complex 1 as the catalyst and H₂O₂ as the oxidant in different solvents.^[a]

| Solvent | t [h] | Conv. [%] ^[b] | Prod. sel. [%] ^[c] | | | % ee ^[d] |
|----------------------------------|-------|--------------------------|-------------------------------|------|--------|---------------------|
| | | | SO | BA | others | |
| CH ₃ OH | 36 | 16.5 | 9.2 | 89.6 | 1.2 | 15 |
| C ₂ H ₅ OH | 36 | 13.2 | 8.9 | 89.4 | 1.7 | 18 |
| CH ₃ CN | 36 | 66.2 | 76 | 22.2 | 1.8 | 32 |
| CH ₂ Cl ₂ | 36 | 30.2 | 52 | 48 | – | 22 |
| DMF | 36 | 31.5 | 68 | 32 | – | 27 |
| CHCl ₃ | 36 | 14.3 | 62 | 38 | – | 29 |
| H ₂ O | 36 | 34.2 | 2.2 | 85.6 | – | 16 |
| toluene | 36 | – | – | – | – | – |
| hexane | 36 | – | – | – | – | – |

[a] Reaction conditions: catalyst 10 mg, styrene 5 mmol, solvent 10 mL, 30% H₂O₂ 2 mL, 0 °C. [b] Determined by GC analysis; conversion (%) = [moles of reactant converted] × 100 / [moles of reactant in feed]. [c] Product selectivity (%) = [moles of product formed] × 100 / [moles of reactant converted]. [d] Selectivity for the R product; determined by HPLC analysis on a chiral stationary phase.

oxidation of styrene was slow with less conversion and poor selectivity towards epoxidation. Liu et al.^[33] also observed similar solvent effects for epoxidation in the presence of a Au-silica catalyst. In the presence of less polar solvents the oxidation of styrene is better than in protic solvents and also the selectivity towards epoxide formation is improved. Interestingly, the reaction does not proceed in nonpolar solvents such as toluene and hexane, indicating the effect of solvent polarity on the catalytic conversion of styrene to styrene oxide. Of the various solvents considered, the best results were obtained with acetonitrile (CH₃CN): 66% conversion and 76% selectivity (Table 4). Since CH₃CN is found to be a suitable solvent for the epoxidation process, we carried out the oxidation of styrene with all of the synthesized catalysts in CH₃CN.

In order to observe the effect of temperature, we again performed the oxidation of styrene in CH₃CN with complex 1 as the test catalyst over a range of temperatures (Table 5). At room temperature (30 °C) the oxidation was very slow and we obtained benzaldehyde as the major product and styrene oxide with only 5% ee. When the reaction was conducted in an ice bath (0 °C) both the conversion and the selectivity towards epoxidation improved and the enantioselectivity increased to 32% ee. However, on lowering the temperature to –20 °C we observed low conversion, low selectivity, and a slight decrease in enantioselectivity. We attribute the steady increase in enantioselectivity at 0 °C to the formation of a more persistent and a better organized activated complex at lower thermal energy.^[34] Hence, we performed the catalytic oxidation of styrene using all other catalysts at 0 °C. Hutchings and co-workers have also found a decrease in enantioselectivity at –10 °C for the epoxidation of stillbene using Mn salen complexes.^[21]

These results show a clear trend where the sense of induction is reversed in accordance with the Arrhenius law and also improves with decreasing temperature from room temperature to 0 °C. Generally, it is believed that the log rate constant increases with absolute temperature, according to the Arrhenius

Table 5. Oxidation of styrene using complex 1 as the catalyst and H₂O₂ as the oxidant at different reaction temperatures.^[a]

| T [°C] | 1/T [K ⁻¹] × 10 ⁻³ | t [h] | Conv. ^[b] [%] | Prod. sel. [%] ^[c] | | | % ee ^[d] | ln [K _S /K _R] |
|--------|--|-------|-----------------------------|-------------------------------|------|--------|---------------------|--------------------------------------|
| | | | | SO | BA | others | | |
| 30 | 3.30 | 36 | 6.5 | 2.2 | 79.6 | 18.2 | 5 | 1.24 |
| 20 | 3.41 | 36 | 9.2 | 8.9 | 76.4 | 14.7 | 17 | 2.34 |
| 5 | 3.59 | 36 | 26.2 | 46 | 35 | 19 | 22 | 1.99 |
| 0 | 3.6 | 36 | 66.2 | 76 | 22.2 | 1.8 | 32 | 2.21 |
| -5 | 3.73 | 36 | 54.5 | 52 | 32 | 16 | 30 | 2.76 |
| -10 | 3.80 | 36 | 44.3 | 42 | 38 | 20 | 29 | 2.56 |
| -20 | 3.95 | 36 | 39.2 | 28 | 51 | 11 | 26 | 2.00 |

[a] Reaction conditions: catalyst 10 mg, styrene 5 mmol, solvent 10 mL, 30% H₂O₂ 2 mL. [b] Determined by GC analysis; conversion (%) = [moles of reactant converted] × 100 / [moles of reactant in feed]. [c] Product selectivity (%) = [moles of product formed] × 100 / [moles of reactant converted]. [d] Selectivity for the R product; determined by HPLC analysis on a chiral stationary phase.

law. This law holds well only if the process continues to follow the same reaction sequence. As the temperature increases, the rate of the reaction will increase but the supply of molecules to the surface will become slow, and accordingly the Arrhenius plot will change slope. In the present case lowering temperature favors the reaction since adsorption and surface concentration is a function of temperature, especially when the molecule has to adsorb in a particular mode to give stereospecificity. Further, when the temperature was lowered from 37 °C to 0 °C, the partition coefficient (*K*) values increased from 3.13 to 3.78. However, a further decrease in temperature decreases the partition coefficient value. Thus the reaction was performed at 0 °C at pH 6.5–6.8.

In order to further substantiate this fact, the natural logarithm of the relative rate constant for the formation of (*S*)- and (*R*)-styrene oxide can be correlated with the *ee* values of the reaction according to Equation (1), which can also be written as the differential Eyring equation shown in Equation (2).^[35–37]

$$\ln \left[\frac{K_S}{K_R} \right] = \ln \left[\frac{(100 + \%ee)}{(100 - \%ee)} \right] \quad (1)$$

$$\ln \left[\frac{K_S}{K_R} \right] = \frac{-\Delta\Delta H^\ddagger}{RT} = \frac{\Delta\Delta S^\ddagger}{R} \quad (2)$$

Considering Equation (2), a linear plot would be expected if the mechanism of the enantioselection remained constant over a wide range of temperatures. In this case $\Delta\Delta H^\ddagger$ and $\Delta\Delta S^\ddagger$ should remain unchanged. In contrast, a nonlinear curve will result if the enantiodetermining step changes at different temperatures because of the variation in the $\Delta\Delta H^\ddagger$ and $\Delta\Delta S^\ddagger$ values. In the present case the plot of $\ln(K_S/K_R)$ vs $1/T$ shown in Figure S3 is found to be nonlinear. Therefore it appears that the enantiodetermining step is changing over the range of temperatures examined. Thus, the observed reversal in absolute chiral induction could arise from a temperature-dependent interchange of the enantiodetermining mechanisms.

Effect of oxidant concentration and catalyst amount

The effect of the oxidant concentration on the styrene epoxidation was studied by GC analysis and cyclic voltammetry, and again we used complex 1 as the test catalyst. In the GC analysis, in the absence of oxidant we did not observe any signal for the formation of epoxide. However, on sequential addition of H₂O₂ from 0.2 mL to 2 mL, two new additional peaks appeared at retention times of 13.23 and 18.50 min corresponding to epoxide and benzaldehyde (Figure 13). It was observed

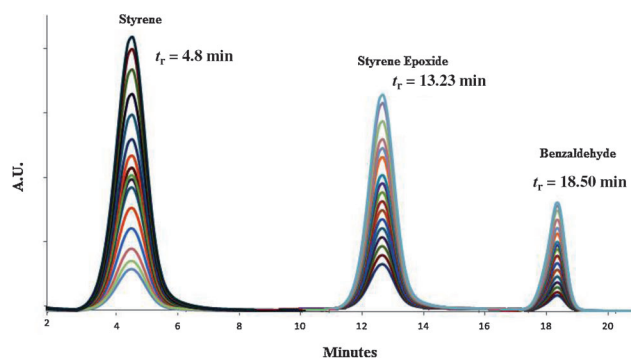


Figure 13. GC analysis showing the effect of peroxide concentration on the oxidation of styrene catalyzed by complex 1.

that as the concentration of H₂O₂ was increased up to 2 mL, the conversions of styrene and epoxidation selectivity also increased. A further increase in H₂O₂ did not lead to further improvements in catalytic conversion, rather the addition of 2.5 mL of H₂O₂ resulted in some unwanted minor products. This indicates that excess oxidant does not have a beneficial effect on oxidation of styrene. Thus, 2 mL of H₂O₂ is considered as the optimum amount of oxidant for the catalytic process. Figure 14a is the cyclic voltammogram recorded for complex 1 with different concentrations of styrene. The concentration of styrene has no any significant effect on the reduction potential of complex 1. However, on addition of H₂O₂, the reduction peak corresponding to Mn^{III} → Mn^{II} vanishes and a new quasi-reversible couple for Mn^{III}/Mn^{IV} and a couple for Mn^{IV}/Mn^{III} couple appear at 0.69 and 0.223 V, respectively (Figure 14b). This indicates that the epoxidation of styrene proceeds through the formation of Mn^{IV}=O species as one of the intermediates.^[38] Cyclic voltammetry studies also suggest that the concentration of H₂O₂ plays a dominant role in the catalytic oxidation of styrene and the epoxidation reaction proceeds through the formation of Mn^{IV}-oxo species.

To investigate the effect of the catalyst amount, we performed the catalytic oxidation of styrene using complex 1 as the test catalyst and H₂O₂ as the oxidant. Keeping the substrate amount fixed (5 mmol) and oxidant amount at 2 mL, we varied the catalyst loading from 0.5 to 25 mg. Increasing the amount of catalyst from 0.5 to 15 mg leads to enhancement in enantioselectivity from 23% to 46% *ee*. Styrene conversion and epoxidation selectivity is found to be highest with 15 mg

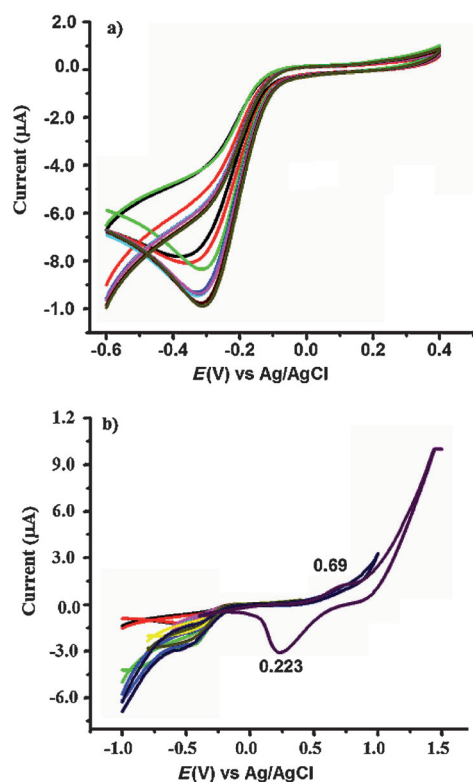


Figure 14. CV study to elucidate the effect of styrene on complex 1 and d) the effect of peroxide.

loading of the catalyst. However, no any enhancement in the catalytic process nor in the enantioselectivity was observed on increasing the catalyst loading to 25 mg. So we considered 15 mg as the effective amount of catalyst for the catalytic oxidation of styrene.

Comparison of catalytic activity of homogeneous and heterogeneous catalyst

After optimization of the solvent, temperature, and oxidant and catalyst concentration, we performed oxidation of styrene using various catalysts under similar conditions. All the chiral catalysts give (*R*)-styrene oxide with some level of enantioselectivity according to HPLC analysis (Table 6). Complex 1 and its heterogeneous counterpart are found to be most effective for catalytic epoxidation of styrene in the presence of hydrogen peroxide. In comparison to complex 1, complex 2 and its heterogeneous counterparts shows poor catalytic activity. The differences in the catalytic activity of the two complexes can be attributed to structural changes caused by the nature of the ligand. The conversion of styrene to styrene epoxide by complex 1 and its heterogeneous counterpart is comparable. However, the reaction takes less time with immobilized catalysts and the enantioselectivity is enhanced (71% *ee* vs. 46% *ee*). It has been reported that the system composed of an aldehyde and a transition metal can effect the aerobic epoxidation of alkenes.^[39,40] So we performed the catalytic epoxidation by adding pyridine carboxaldehyde as an additive to simulate

Table 6. Oxidation of styrene using 15 mg loading of various catalysts and H₂O₂ (2 mL) as the oxidant in CH₃CN at 0 °C.

| Catalyst | t [h] | Conv. [%] ^[a] | Prod. sel. [%] ^[b] | | | % ee [R] ^[c] |
|--|-------|--------------------------|-------------------------------|----|--------|-------------------------|
| | | | SO | BA | Others | |
| H ₂ O ₂ | 26 | 20 | – | 76 | 24 | – |
| Mn(OAc) ₂ ·4H ₂ O | 36 | – | – | – | – | – |
| Mn(OAc) ₂ + H ₂ O ₂ | 24 | 30 | 5 | 78 | 17 | – |
| complex 1 | 36 | – | – | – | – | – |
| complex 2 | 36 | – | – | – | – | – |
| complex 1 + H ₂ O ₂ | 36 | 77 | 82 | 18 | – | 46 |
| complex 2 + H ₂ O ₂ | 42 | 46 | 62 | 38 | – | 38 |
| complex 1 + H ₂ O ₂ + pyridine | 38 | 72 | 84 | 10 | 6 | 67 |
| carboxaldehyde | | | | | | |
| complex 2 + H ₂ O ₂ + pyridine | 40 | 63 | 61 | 28 | 11 | 44 |
| carboxaldehyde | | | | | | |
| complex 1/MCM-41 + H ₂ O ₂ | 27 | 68 | 88 | 12 | – | 71 |
| complex 2/MCM-41 + H ₂ O ₂ | 34 | 57 | 67 | 33 | – | 52 |

[a] Determined by GC analysis; conversion (%) = [moles of reactant converted] × 100 / [moles of reactant in feed]. [b] Product selectivity (%) = [moles of product formed] × 100 / [moles of reactant converted]. [c] Selectivity for the *R* product; determined by HPLC analysis on a chiral stationary phase.

better the environment of the Mn complexes in the solid. We found that under these conditions the enantioselectivity is better than that obtained with the complexes alone and almost comparable to that obtained with the heterogeneous system (Table 6). In a control experiment with H₂O₂, MCM-41, pyridine carboxaldehyde modified MCM-41, Mn(OAc)₂, and H₂O₂, we observed negligible catalytic activity without any selectivity toward the epoxidation of styrene (Table 6). Hence we can conclude that the catalytic activity is entirely attributed to the salen complex in both the homogeneous phase and also immobilized on the pyridine carboxaldehyde modified MCM-41.

Recyclability test

The homogeneous complexes could not be retrieved, whereas we could successfully recover the MCM-41-supported chiral catalyst. In recent years ionic liquids have been used recovering homogeneous catalysts.^[41,42] We have also reported the successful recovery of a chiral Cu^{II} Schiff base complex in an asymmetric Henry reaction.^[16] So, in order to recover the chiral catalyst we implemented ionic liquid 1-butyl-3-methylimidazolium hexafluorophosphate [BMIM][PF₆]. In the presence of the ionic liquid we do not observe any change in catalytic conversion and selectivity. But we could recover the catalyst and used it in two consecutive cycles without any loss in catalytic activity. After the third cycle sufficient metal leaching has probably occurred; a UV/Vis study indicates that the metal complexes are ruptured. The UV/Vis spectrum of the recovered catalyst does not show any band characteristics of complex 1 and complex 2 and indicates that the structure has been destroyed (Figures S4 and S5). To study the recyclability of the immobilized catalyst during epoxidation of styrene, we carried out a few epoxidation reactions with complex 1/MCM-41 and complex 2/MCM-41. After the first run, the catalyst was removed by centrifugation. Fresh reactants were added to the supernatant. Analysis of the

reaction mixture by gas chromatography shows no further increase in the conversion of styrene. UV/Vis analysis of the supernatant also indicated an absence of trace amounts of the metal complex. After separation, the catalyst was washed thoroughly with dichloromethane (DCM), dried, and subjected to another cycle with fresh reactants under similar epoxidation conditions. Epoxide conversion, yield, and enantioselectivity were found to be consistent. The above procedure was repeated for five cycles, and we did not observe any substantial loss in the catalytic activity of the immobilized catalyst. This indicates that the chiral Mn^{III} salen complex is strongly bonded to the nitrogen atom of pyridine carboxaldehyde modified MCM-41 through the axial coordination. However, after the fifth cycle, that is, in sixth and seventh cycle, we observed a substantial decrease in the catalytic activity.

To determine the reason for the loss in catalytic activity we performed an EPR analysis. EPR spectra of the two Mn complexes were recorded in the solid phase at 77 K after the sixth and seventh cycle (Figure 15 a–d). They show the usual Mn^{II} ($S=5/2$) six-line hyperfine pattern assigned to the $\Delta M_I=0$ spin-allowed transitions. Both chiral complexes exhibit an intense signal at $g=2.10$ with the partially resolved hyperfine splitting (10 mT or 10 G) from the manganese nucleus. The presence of the six-line hyperfine signal at $g=2.10$ with $A=10$ mT indicates that in both the complexes the metal ions have leached out as Mn²⁺ ions.^[43] It is interesting to see that intensity of the EPR signal after the fifth run is less than after sixth cycle. This further indicates that after sixth cycle amount of Mn²⁺ on the surface of MCM-41 increases due to metal leaching.

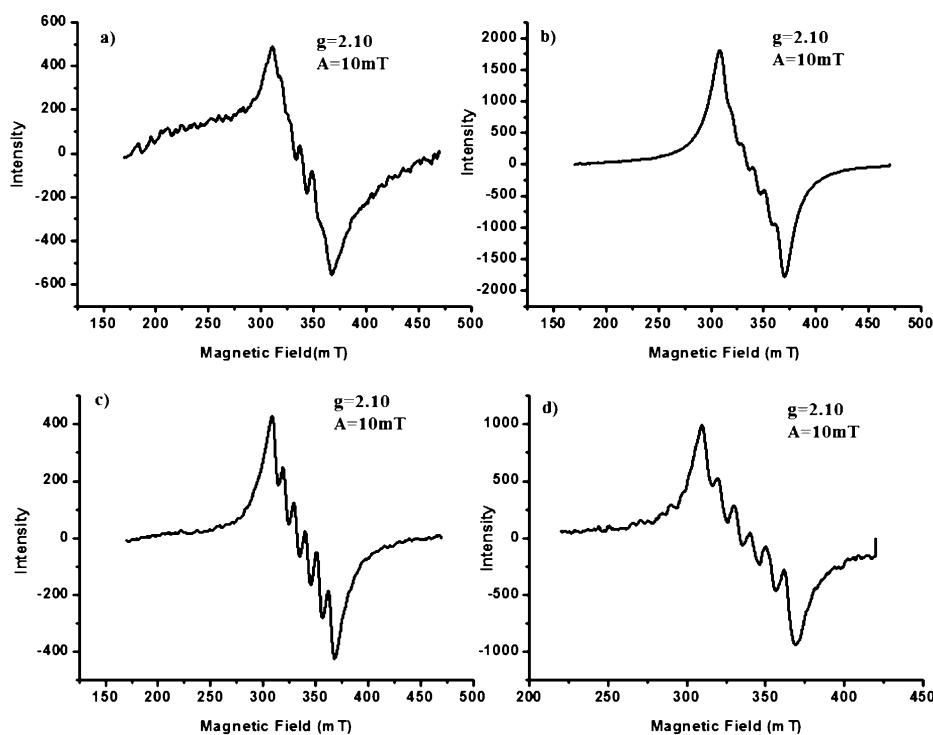


Figure 15. EPR spectra of a) complex 1/MCM-41, b) complex 2/MCM-41 after the fifth cycle (c) and after the sixth cycle (d), respectively.

Conclusion

In conclusion we have successfully synthesized two chiral Mn Schiff base complexes and they have been characterized by various spectrochemical and physicochemical techniques. The two complexes are immobilized on MCM-41 using linkers. The homogeneous and heterogeneous catalysts are found to be effective catalysts for oxidation of styrene. The heterogeneous catalysts show activity similar to that of the homogeneous catalysts. Upon immobilization, the conversion and enantioselectivity are enhanced. The use of an ionic liquid does not affect the catalytic results but has provided a suitable means to recycle the homogeneous catalyst up to three consecutive cycles. Upon immobilization on MCM-41, the catalysts can be successfully recycled up to five times without loss of catalytic activity. An EPR study indicates that the heterogeneous systems is deactivated due to loss of manganese as Mn²⁺.

Experimental Methods

Preparation of Schiff base ligands

6,6''-(1,2-Diphenylethane-1,2-diyl)bis(azan-1-yl-1-ylidene)bis(methan-1-yl-1-ylidene)bis(3-methoxyphenol) (ligand 1)

Ligand 1 was prepared by stirring a solution of (1*R*,2*R*)-(+)-1,2-diphenylethylenediamine (424 mg, 2 mmol) and 2-hydroxy-4-methoxybenzaldehyde (608 mg, 4 mmol) at room temperature for 18 h under nitrogen atmosphere in ethanol, (Scheme 1). After completion of the reaction, the reaction mixture was diluted with EtOAc and water. The organic layer was then separated and washed sequentially with brine and dried over Na₂SO₄. The solvent was removed in vacuum and the resulting residue was purified by chromatography. TLC was conducted with 10% EtOAc and hexane. Ligand 1 was eluted with 6% EtOAc in hexane. $R_f=0.4$.

¹H NMR (300 MHz, CDCl₃): $\delta=13.83$ (s, 1H), 8.17 (s, 1H), 7.19 (m, 5H), 7.01 (d, $J=9.06$ Hz, 1H), 6.45 (d, $J=2.26$ Hz, 1H), 6.35 (dd, $J=2.26, 9.06$ Hz, 1H), 4.65 (s, 1H), 3.78 (s, 3H). ¹³C NMR (75 MHz, CDCl₃): $\delta=165.06, 163.60, 163.28, 139.60, 132.81, 128.19, 127.72, 127.38, 112.36, 106.28, 100.96, 79.55, 55.15$

2,2'-(Cyclohexane-1,2-diyl)bis(azan-1-yl-1-ylidene)bis(methan-1-yl-1-ylidene)diphenol (ligand 2)

Ligand 2 was prepared analogously using a solution of

(1*R*,2*R*)-(–)-1,2-diaminocyclohexane (456 mg, 8 mmol) and 2-hydroxybenzaldehyde (1.952 g, 1.7 mL, 16 mmol) in ethanol (Scheme 1).

¹H NMR (500 MHz, CDCl₃): δ = 13.26 (s, 1 H), 8.23 (s, 1 H), 7.22 (t, *J* = 7.72, 6.62 Hz, 1 H), 7.12 (d, *J* = 7.72 Hz, 1 H), 6.87 (d, *J* = 7.72 Hz, 1 H), 6.77 (t, *J* = 7.72, 6.62 Hz, 1 H), 3.29 (dd, *J* = 9.93, 4.41 Hz, 1 H), 1.4–1.94(m, 4 H). ¹³C NMR (75 MHz, CDCl₃): δ = 164.65, 160.92, 132.10, 131.42, 118.60, 118.53, 116.72, 72.57, 33.04, 24.13.

Preparation of Mn^{III} Schiff base complexes (complex 1 and complex 2)

To a well-stirred solution of 1 mmol of either ligand 1 or ligand 2 in 10 mL methanol, 1 mmol of Mn(OAc)₂·4H₂O (0.245 g, 1 mmol) was added. The homogeneous solution was stirred for 3 h and kept for crystallization. The dark brown crystals so obtained were washed with ethanol and diethyl ether and finally dried at room temperature (Scheme 1).

Preparation of immobilized chiral metal complexes

MCM-41-supported chiral manganese complexes were synthesized according to the stepwise process shown in Scheme 2. A suspension of 2 g of MCM-41 and 0.3 g of 3-aminopropyltrimethoxysilane and in 20 mL of toluene was refluxed at 80 °C with constant stirring for 24 h. The resulting solution was cooled to room temperature and a white solid was collected after 1 h. The powder was filtered and washed with diethyl ether. The solid white product was finally dried under vacuum for 12 h. To this amino-functionalized MCM-41, 2 mmol of 4-pyridine carboxaldehyde was added and the reaction mixture stirred at 75 °C for 16 h to obtain compound 2, pyridine carboxaldehyde modified MCM-41. In separate experiments solutions of complex 1 and complex 2 (1 mmol) in ethanol (10 mL) were added to pyridine carboxaldehyde modified MCM-41 (1 g), and the resulting suspensions were refluxed for 48 h. The immobilized catalysts 3 and 4 were filtered, washed thoroughly with anhydrous toluene, and extracted repeatedly with methanol and dichloromethane on a Soxhlet extractor until the extracted liquid became colorless.

The above-mentioned strategy to anchor the metal complexes through apical co-ordination over MCM-41 was used taken because heterogenization can be also advantageous from the point of view of catalyst stability, as immobilization frequently improves catalyst stability compared to the homogeneous analogues. This stabilization can be attributed to steric constraints and site isolation that minimize complex degradation.^[15]

General procedure for oxidation of styrene

The enantioselective epoxidation of styrene was carried out with synthesized homogeneous and heterogeneous catalysts (15 mg) using 5 mmol of the substrate in 10 mL of acetonitrile and 2 mL of 30% H₂O₂ at 0 °C.

Acknowledgements

We thank Debabrata Singha (Debu), Research Scholar, IIT, Guwahati, for providing ESR analysis and Prof. B. Viswanathan, National Centre for Catalysis Research (NCCR), IIT Madra, for fruitful discussions.

Keywords: ionic liquids • manganese • MCM-41 • styrene oxidation • Schiff base complexes

- [1] H. Mihara, Y. Xu, N. E. Shepherd, S. Matsunaga, M. Shibusaki, *J. Am. Chem. Soc.* **2009**, *131*, 8384–8385.
- [2] T. Tanaka, Y. Yasuda, M. Hayashi, *J. Org. Chem.* **2006**, *71*, 7091–7093.
- [3] Y. Y. Kato, M. Furutachi, Z. Chen, H. Mitsunuma, S. Matsunaga, M. Shibusaki, *J. Am. Chem. Soc.* **2009**, *131*, 9168–9169.
- [4] R. T. Ruck, E. N. Jacobsen, *J. Am. Chem. Soc.* **2002**, *124*, 2882–2883.
- [5] P. S. Dixit, K. Srinivasan, *Inorg. Chem.* **1988**, *27*, 4507–4509.
- [6] D. E. De Vos, M. Dams, B. F. Sels, P. A. Jacobs, *Chem. Rev.* **2002**, *102*, 3615–3640.
- [7] W. F. Beyer Jr., I. Fridovich, *Manganese in Metabolism and Enzyme Function*, Academic Press, New York, **1986**, chap. 12, p. 193.
- [8] E. N. Jacobsen in *Comprehensive Organometallic Chemistry II*, Vol. 12 (Eds.: E. W. Abel, F. G. A. Stone, E. Wilkinson), Pergamon, Oxford, **1995**, p. 1097.
- [9] T. Katsuki, *J. Mol. Catal. A: Chem.* **1996**, *113*, 87–107.
- [10] D. D. Agarwal, R. P. Bhatnagar, R. R. Jain, S. Srivastava, *J. Chem. Soc. Perkin Trans. 2* **1990**, 989–992.
- [11] M. D. Godbole, A. C. G. Hotze, R. Hage, A. M. Mills, H. H. Kooijman, A. L. Spek, E. Bouwman, *Inorg. Chem.* **2005**, *44*, 9253–9266.
- [12] W. Adam, H. U. Humpf, K. J. Roschmann, C. R. S. Möller, *J. Org. Chem.* **2001**, *66*, 5796–5800.
- [13] J. G. de Vries, S. D. Jackson, *Catal. Sci. Technol.* **2012**, *2*, 2009–2009.
- [14] P. W. N. M. van Leeuwen, *Appl. Catal. A* **2001**, *212*, 61–81.
- [15] C. Baleizão, H. Garcia, *Chem. Rev.* **2006**, *106*, 3987–4043.
- [16] K. K. Bania, G. V. Karunakar, B. Sarma, R. C. Deka, *ChemPlusChem* **2014**, *79*, 427–438.
- [17] C. Li, H. Zhang, D. Jiang, Q. Yang, *Chem. Commun.* **2007**, 547–558.
- [18] K. K. Bania, D. Bharali, B. Viswanathan, R. C. Deka, *Inorg. Chem.* **2012**, *51*, 1657–1674.
- [19] D. J. Cole-Hamilton, *Science* **2003**, *299*, 1702–1706.
- [20] B. M. L. Dioso, P. A. Jacobs, *Tetrahedron Lett.* **2003**, *44*, 8815–8817.
- [21] P. Piaggio, P. McMorn, D. Murphy, D. Bethell, P. C. B. Page, F. E. Hancock, C. Sly, O. J. Kerton, G. J. Hutchings, *J. Chem. Soc. Perkin Trans. 2* **2000**, 2008–2015.
- [22] D. J. Xuereb, R. Raja, *Catal. Sci. Technol.* **2011**, *1*, 517–534.
- [23] J. M. Thomas, R. Raja, *Acc. Chem. Res.* **2008**, *41*, 708–720.
- [24] M. E. Davis, *Nature* **2002**, *417*, 813–821.
- [25] P. Piaggio, P. McMorn, C. Langham, D. Bethell, P. C. B. Page, F. E. Hancock, G. J. Hutchings, *New J. Chem.* **1998**, 1167–1169.
- [26] R. I. Kureshy, I. Ahmad, N. H. Khan, S. H. R. Abdi, K. Pathak, R. V. Jasra, *J. Catal.* **2006**, *238*, 134.
- [27] D. Zhao, J. Zhao, S. Zhao, W. Wang, *J. Inorg. Organomet. Polym.* **2007**, *17*, 653–659.
- [28] R. I. Kureshy, I. Ahmad, N. H. Khan, S. H. R. Abdi, S. Singh, P. H. Pandia, R. V. Jasra, *J. Catal.* **2005**, *235*, 28–34.
- [29] J. A. Bonadies, M. L. Kirk, M. S. Lah, D. P. Kessiosoglou, W. E. Hatfield, V. L. Pecoraro, *Inorg. Chem.* **1989**, *28*, 2037–2044.
- [30] R. Schmidt, E. W. Hansen, M. Stoecker, D. Akporiaye, O. H. Ellestad, *J. Am. Chem. Soc.* **1995**, *117*, 4049–4056.
- [31] J. A. Bonadies, M. J. Maroney, V. L. Pecoraro, *Inorg. Chem.* **1989**, *28*, 2044–2051.
- [32] A. Doménech, M. Alvaro, B. Ferrer, H. García, *J. Phys. Chem. B* **2003**, *107*, 12781–12788.
- [33] J. Liu, F. Wang, S. Qi, Z. Gua, G. Wuc, *New J. Chem.* **2013**, *37*, 769–774.
- [34] A. N. Thadani, A. R. Stankovic, V. H. Rawal, *Proc. Natl. Acad. Sci. USA* **2004**, *101*, 5846–5850.
- [35] J. Otera, K. Sakamoto, T. Tsukamoto, A. Orita, *Tetrahedron Lett.* **1998**, *39*, 3201–3204.

- [36] R. Saito, S. Naruse, K. Takano, K. Fukuda, A. Katoh, Y. Inoue, *Org. Lett.* **2006**, *8*, 2067–2070.
- [37] V. S. Chan, M. Chiu, R. G. Bergman, F. D. Toste, *J. Am. Chem. Soc.* **2009**, *131*, 6021–6032.
- [38] W. Adam, C. M. Knoblauch, C. R. S. Mo1ler, M. Herderich, *J. Am. Chem. Soc.* **2000**, *122*, 9685–9691.
- [39] T. Yamada, K. Imagawa, T. Mukaiyama, *Chem. Lett.* **1992**, 2109–2112.
- [40] A. Dhakshinamoorthy, M. Alvaro, H. Garcia, *ACS Catal.* **2011**, *1*, 836–840.
- [41] N. Audic, H. Clavier, M. Mauduit, J. C. Guillemin, *J. Am. Chem. Soc.* **2003**, *125*, 9248–9249.
- [42] a) P. Wasserscheid, W. Keim, *Angew. Chem. Int. Ed.* **2000**, *39*, 3772–3789; *Angew. Chem.* **2000**, *112*, 3926–3945; b) J. Dupont, R. F. de Souza, P. A. Z. Suarez, *Chem. Rev.* **2002**, *102*, 3667–3692.
- [43] K. P. Bryliakov, D. E. Babushkin, E. P. Talsi, *Mendeleev Commun.* **1999**, *9*, 29–31.

Received: December 17, 2014

Revised: January 19, 2015

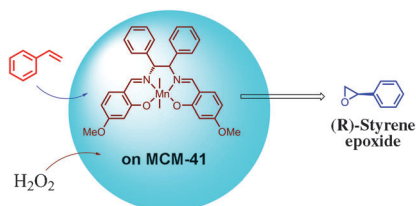
Published online on ■ ■ ■, 0000

FULL PAPERS

M. Mandal, V. Nagaraju, B. Sarma,
G. V. Karunakar, K. K. Bania*



Enantioselective Epoxidation of Styrene by Manganese Chiral Schiff Base Complexes Immobilized on MCM-41



Thanks for the support! Chiral Mn^{III} Schiff base complexes were attached to mesoporous silica MCM-41. Although both the homogeneous and heterogeneous versions were effective catalysts for the epoxidation of styrene, the supported catalysts retained their catalytic activity for up to five cycles.